Applied Catalysis B: Environmental 158–159 (2014) 129–135

Contents lists available at ScienceDirect

Applied Catalysis B: Environmental

journal homepage: www.elsevier.com/locate/apcatb

Silver nanoparticles immobilized on fibrous nano-silica as highly efficient and recyclable heterogeneous catalyst for reduction of 4-nitrophenol and 2-nitroaniline

Zhengping Dong*, Xuanduong Le, Xinlin Li, Wei Zhang, Chunxu Dong, Jiantai Ma

College of Chemistry and Chemical Engineering, Gansu Provincial Engineering Laboratory for Chemical Catalysis, Lanzhou University, Lanzhou 730000, PR China

ARTICLE INFO

Article history:
Received 10 February 2014
Received in revised form 26 March 2014
Accepted 8 April 2014
Available online 18 April 2014

Keywords:
Fibrous nano-silica
Ag/KCC-1 nanocatalyst
Easy accessibility
Reduction
Nitro-compounds

ABSTRACT

In this study, a novel fibrous nano-silica (KCC-1) based nanocatalyst (Ag/KCC-1) with high surface area and easy accessibility of active sites was successfully developed by a facile approach. KCC-1 with high surface area was functionalized with amino groups acting as the robust anchors so that the silver nanoparticles (Ag NPs) with average diameter of about 4 nm were well-dispersed on the fibers of the KCC-1 microspheres, without aggregation. The synthesized Ag/KCC-1 nanocatalyst exhibited excellent catalytic activity for the reduction of 4-nitrophenol and 2-nitroaniline using sodium borohydride ($NaBH_4$) in water at room temperature owing to the easy accessibility of the active sites. Importantly, the Ag/KCC-1 nanocatalyst was easily recovered and reused for at least ten cycles in both the reduction reactions; thus, confirming its good stability. The enhanced stability was attributed to the modification of the fibrous nature of KCC-1 by the amino groups; thus, restricting Ostwald ripening and leaching of Ag NPs. Therefore, the abovementioned approach based on fibrous KCC-1 provided a useful platform for the fabrication of noble metal nanocatalysts with easy accessibility, which would be highly efficient in various catalytic reductions.

1. Introduction

Recently, green chemistry has attracted considerable attention to overcome the problem pertaining to the environmental pollution being encountered by the global population. The processes avoiding the use of organic solvents for the transformation of harmful organic wastes into reusable compounds with low toxicity in aqueous solutions under mild condition are extremely significant for the chemists. In this aspect, the disposal of nitroaromatic compounds is an area of intensive research, recently [1–6]. Nitrophenols (NP) are among the most common organic pollutants in industrial and agricultural wastewaters. In particular, 4-NP is a notorious industrial pollutant exhibiting high solubility and stability in water [7,8]. Moreover, even low concentration of 2-nitroaniline (2-NA) in water is harmful to aquatic life and human health in terms of its toxicity, and potential carcinogenic and mutagenic effects [9,10]. Therefore, the Unites States Environmental Protection Agency has listed 4-NP and 2-NA as hazardous wastes and priority toxic pollutants. It is therefore important to develop effective methods for their removal. Till date, various processes have been developed for the disposal of these nitro-compounds including microbial degradation, photocatalytic degradation, microwave-assisted catalytic oxidation, electro-Fenton method, electrocoagulation, and electrochemical treatment [11–13]. However, the reduction of nitro group to amino group is considered to be the most efficient, green, and economical approach to dispose nitro-compounds [14–18], and the reduction products namely, 4-aminophenol (4-AP) and *o*-phenylenediamine (*o*-PDA) can be reused because they are important intermediates for the synthesis of drugs and dyes [9,19]. Therefore, development of low-cost, stable, and highly effective catalyst for the reduction of nitro-compounds in aqueous solutions under mild condition is highly desirable.

Noble metal nanoparticles (NPs) have attracted significant attention in catalysis science due to their high efficiency as heterogeneous catalysts in numerous liquid-phase catalytic processes [20–26]. The catalytic activity of NPs is strongly dependent on the active atoms on the surface that are usually related to the specific surface area, surface structure, and edges of the catalysts [27–29]. Smaller NPs exhibit superior catalytic activities because of their higher surface-to-volume ratio. However, stability of metallic NPs

* Corresponding author. Tel.: +86 0931 8912577; fax: +86 0931 8912582.
E-mail addresses: dongzhp@lzu.edu.cn (Z. Dong), majiantai@lzu.edu.cn (J. Ma).

http://dx.doi.org/10.1016/j.apcatb.2014.04.015
0926-3373/

is another crucial issue for their further application. The surface energy of NPs increases with decrease in the particle size; thus, making them unstable leading to high tendency for inter-particle aggregation [30]. This eventually reduces catalytic efficiency of the catalysts. In order to control their catalytic properties, the catalytically active metal NPs are usually immobilized on the solid supports with mesopores such as SBA-15 [31,32], Al_2O_3 [33–35] and MCM-41[36–38] regarded as ideal supports for heterogeneous catalyst due to their excellent stability, high surface area, tunable pore size, and robust surface chemistry. The effectiveness of these materials as catalyst supports is attributed to the dispersion of the active catalytic sites on the large specific surface areas and pores, which in turn prevent the aggregation of NPs and improve the activity of the catalyst system. However, poor accessibility to these active sites inside the pores limits their applications for which significant mass transport is essential. Therefore, silica supports with easily accessible high surface areas, not due to the pores, are needed. Vivek Polshettiwar reported the fabrication of fibrous silica nanospheres (KCC-1) with easily accessible high surface area attributed to its fibers and not pores [39,40]. Therefore, the unique property of KCC-1 is extremely useful for the design of silica-supported catalysts, for which the accessibility of active sites can be increased significantly.

Inspired by the abovementioned considerations, this study aimed to develop novel catalysts with well-dispersed noble metal NPs and high accessibility, for the catalytic reduction of 4-NP and 2-NA by an eco-friendly approach. Silver (Ag) is relatively cheap compared to other noble metals such as gold (Au), palladium (Pd), and platinum (Pt). Moreover, Ag is non-toxic and eco-friendly. Thus, in this study, KCC-1 was used as the supporting material to stabilize Ag nanoparticles (Ag NPs) to obtain Ag/KCC-1 nanocatalyst with enhanced accessibility for active sites and high surface area. This novel catalyst displayed not only suitable catalytic reaction rate, but also excellent reusability in the catalytic reaction of 4-NP and 2-NA. The robust activity of this catalyst is attributed to its high accessibility and low likelihood of the aggregation of the Ag NPs on the KCC-1 nano-silica support system. Thus, Ag NPs immobilized on KCC-1 exhibited highly effective catalytic property, showing promising potential for the catalytic reduction of nitroaromatic compounds leading to their safe and eco-friendly disposal.

2. Experimental

2.1. Materials

Tetraethyl orthosilicate (TEOS), 3-aminopropyltriethoxysilane (3-APTES), 4-NP, and 2-NA were purchased from Sigma Aldrich and used as received. Reagent-grade cyclohexane, pentanol, cetylpyridinium bromide (CPB), and sodium borohydride ($NaBH_4$) were purchased from Tianjing Guangfu Chemical Company and used as supplied. All other reagents and solvents were used without further purification.

2.2. Preparation of KCC-1

Vivek Polshettiwar reported the synthesis of KCC-1 by the microwave assisted hydrothermal technique [39]. However, in this study, KCC-1 was successfully synthesized by hydrothermal method instead of microwave assisted technique. The detailed experimental procedure was similar to the microwave assisted hydrothermal method. TEOS (2.5 g, 0.012 mol) was dissolved in a solution of cyclohexane (30 mL) and pentanol (1.5 mL) followed by the addition of a stirred solution of CPB (1 g, 0.0026 mol) and urea (0.6 g, 0.01 mol) in water (30 mL). The mixture so obtained was stirred for 30 min at room temperature, and the resulting solution was placed in a teflon-sealed hydrothermal reactor and heated at 120 °C for 5 h. After completion of the reaction, the mixture was cooled to room temperature and the silica so obtained was isolated by centrifugation, washed with distilled water and acetone, and finally dried overnight in a vacuum drying oven. The as-synthesized material was then calcined at 550 °C for 6 h in air to obtain KCC-1.

2.3. Preparation of Ag/KCC-1 nanocatalyst

The synthetic procedure for Ag/KCC-1 nanocatalyst is outlined in Scheme 1. KCC-1 was modified using 3-APTES by the following method: KCC-1 (1 g) and 3-APTES (0.3 g) were mixed in toluene (100 mL) and refluxed with stirring for 12 h under nitrogen atmosphere. White solid of aminopropylfunctionalized KCC-1 (H_2N-KCC-1) thus obtained was centrifuged, washed successively with chloroform, dichloromethane, and ethanol; and finally dried in vacuum. H_2N-KCC-1 (0.5 g) was ultrasonically dispersed in H_2O (50 mL), and subsequently $AgNO_3$ (0.1 g) was added. After being stirred for about 30 min, excess amount of $NaBH_4$ solution was added dropwise. Then the Ag NPs were formed and anchored on the aminopropylfunctionalized fibrous silica. Thus, the Ag/KCC-1 nanocatalyst was obtained by centrifugation and finally dried in vacuum.

2.4. General procedure for the reduction of 4-NP and 2-NA

4-NP was reduced by the following procedure: aqueous 4-NP solution (2.5 mL, 0.12 mM) was mixed with freshly prepared aqueous $NaBH_4$ solution (0.5 mL, 0.5 M) resulting in the formation of deep yellow solution. Subsquently, Ag/KCC-1 catalyst (20 μL, 10 mg mL^{-1}) was added to the yellow solution. The solution became colorless upon the completion of the reaction. For catalytic reduction of 2-NA, aqueous suspension of Ag/KCC-1 catalyst (30 μL, 10 mg mL^{-1}) was added in H_2O (2.8 mL), and then mixed with 2-NA aqueous solution (40 μL, 1.26×10^{-2} mol L^{-1}) and $NaBH_4$ (0.13 mL, 0.5 M) solution was injected rapidly with stirring. The color of the mixture vanished gradually, indicating the reduction of 2-NA. For both the abovementioned reduction reactions, the ambient temperature was maintained at 20 °C. Progress of the reaction was monitored by measuring the UV–Vis absorption spectra of the reaction mixture.

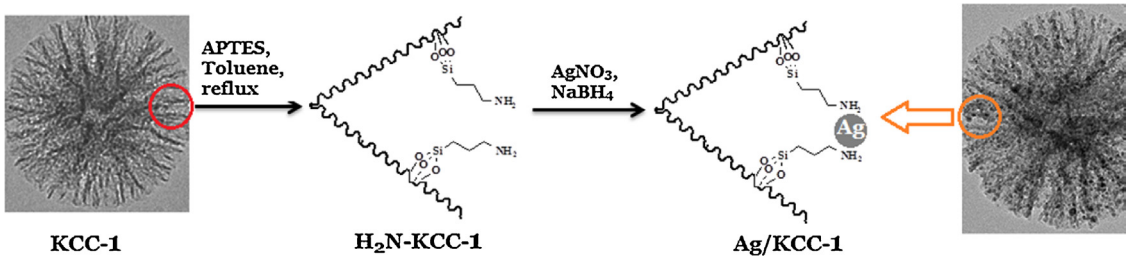

Scheme 1. Synthesis of Ag/KCC-1 nanocatalyst.

After the completion of the reduction reactions, Ag/KCC-1 nanocatalyst was recovered by centrifugation and then washed with water and dried in vacuum at room temperature for the next catalytic run. The aforementioned procedure was repeated ten times.

2.5. Characterization

The size and morphology of the Ag/KCC-1 nanocatlyst were investigated by a Tecnai G^2 F^{30} transmission electron microscopy (TEM). The samples for TEM were prepared by placing a drop of colloidal solution onto a copper grid and evaporating the solvent in air at room temperature. X-ray diffraction (XRD) measurements were performed on a Rigaku D/max-2400 diffractometer using Cu-Kα radiation as the X-ray source in the 2θ range of 10–90°. X-ray photoelectron spectroscopy (XPS) was recorded on a PHI-5702 and the C1S line at 291.4 eV was used as the binding energy (BE) reference. Thermal gravimetric analysis (TGA) was measured under nitrogen atmosphere at 700 °C with a perkin elmer thermal analyzer at a heating rate of 10 °C min^{-1}. Bruker IFS66/S Fourier transform infrared (FTIR) spectrometer was used to obtain the FTIR spectra of KCC-1 and H_2N-KCC-1. The nitrogen adsorption/desorption experiments were performed at 77 K in a micromeritics ASAP 2010 (USA). Elemental analysis (Gmbh Vario El Elementar) and inductively coupled plasma (ICP, IRIS Advantage analyzer) were employed to measure the N, C, H, and Ag content of the samples. Ultraviolet–Visible (UV–Vis) absorption spectra were recorded by a Shimadzu UV 2100 PC UV–visible spectrophotometer.

3. Results and discussion

3.1. Catalysts characterization

The synthesis of Ag/KCC-1 nanocatalysts involved several steps (Scheme 1). The fibers of KCC-1 has many Si–OH groups on the surfaces; thus, it was expected that the KCC-1 could be easily functionalized with 3-APTES to form H_2N-KCC-1. Furthermore, the amino groups on the H_2N-KCC-1 could serve as aggregation centers for the growth of Ag NPs on the surface of KCC-1 [41]. The FTIR spectra of KCC-1 and H_2N-KCC-1 has been displayed in Fig. 1a. The bands at 3200–3500 and 1630 cm^{-1} are attributed to the Si-OH stretching and water molecules absorbed on the KCC-1 surface, respectively. In the two samples, the typical Si–O–Si bands around 1095 and 802 cm^{-1} associated with the formation of a condensed silica network are present. Compared to the spectrum of KCC-1, the peak at 2927 cm^{-1} appearing in the H_2N-KCC-1 corresponds to the stretching vibration saturated C–H on the aminopropyl groups. The results demonstrated the presence of aminopropyl groups on the surface of KCC-1. The TGA (Figure S1) and elemental analysis (Table S1) revealed that the content of 3-APTES grafted onto the surface of KCC-1 was 0.38 mmol g^{-1}. And the aminopropyl groups could provid binding sites for the adsorption of Ag^+ ions on the nanosilica. Ag^+ ions with empty orbital were considered to be rapidly adsorbed; thus, surrounding the amino groups through electrostatic interaction because of the presence of lone pair of electrons on the nitrogen atoms of the amino groups. The addition of $NaBH_4$ led to the rapid reduction of Ag^+ ions and subsequent formation of Ag NPs. ICP analysis revealed that the content of Ag NPs loaded on the surface of KCC-1 was about 8.97% (Table S1). Moreover, the surface areas of KCC-1 and Ag/KCC-1 nanocatalyst calculated from the nitrogen adsorption-desorption were about 459.08 and 281.2 m^2 g^{-1} (Table S1), respectively, indicating the high surface area of the nanocatalyst.

The XRD analysis of KCC-1 and Ag/KCC-1 nanocatalyst is shown in Fig. 1b. The wide hump in the range of 2θ from 15 to 30° was

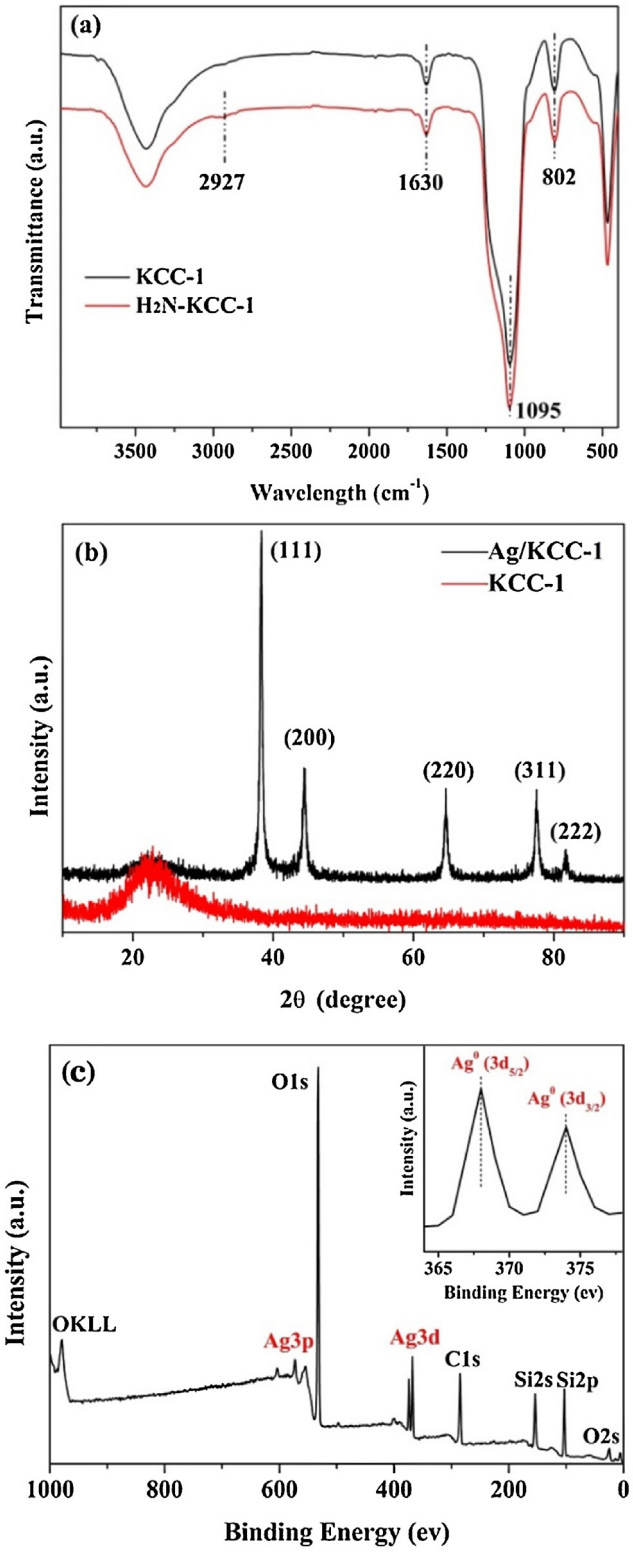

Fig. 1. (a) FTIR spectra of KCC-1 and H_2N-KCC-1, (b) XRD pattern of KCC-1 and Ag/KCC-1, (c) XPS wide-scan spectrum of the Ag/KCC-1 (*inset*: XPS spectrum of Ag 3d).

characteristics of the amorphous silica of KCC-1. After modification of KCC-1 using Ag NPs, five peaks were observed at 2θ = 38.5, 44.3, 64.6, 77.6, and 81.8° corresponding to (1 1 1), (2 0 0), (2 2 0), (3 1 1), and (2 2 2) diffractions from the face-centered cubic structure of Ag NPs (JCPDS No. 00-004-0783). XPS was employed to examine

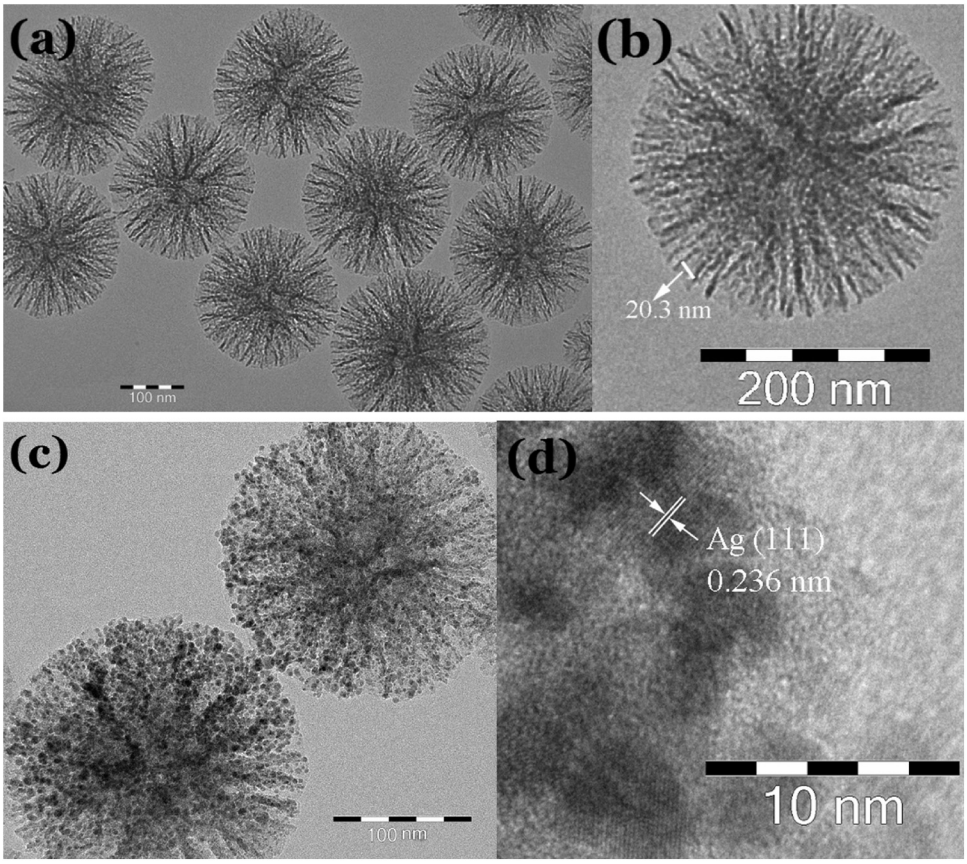

Fig. 2. (a) and (b) HRTEM images of KCC-1, (c) HRTEM image of Ag/KCC-1, (d) HRTEM image of the Ag nanoparticles crystal structure.

the valence states of Ag on the surface of Ag NPs (Fig. 1c). The XPS elemental survey scan of the surface of Ag/KCC-1 nanocatalyst microspheres revealed the presence of silicon, oxygen, silver, and carbon elements in the samples. As shown in Fig. 1c *instet*, the peaks observed in the XPS spectra of Ag 3d at BEs of 368 and 374 eV are characteristic of metallic Ag NPs [31].

The structures of the synthesized KCC-1 and Ag/KCC-1 nanocatalyst were analyzed by TEM. The as-prepared KCC-1 microspheres with fibrous structure were uniform and monodispersed (Fig. 2a). The average diameter of the microspheres was about 200 nm. The high-resolution transmission electron microscopy (HRTEM) image shown in Fig. 2b further clarifies that the distance between the two fibers is about 20 nm (Fig. 2b). The larger distance between the fibers and the high surface area of KCC-1 (Table S1) lead to the easy loading of the Ag NPs on KCC-1, resulting in the significant increase in the accessibility of the active sites on Ag/KCC-1 nanocatalyst. TEM and HRTEM images of the samples of Ag/KCC-1 nanocatalyst are shown in Fig. 2c and d. The Ag NPs with average diameter of about 4 nm were remarkably dispersed on the surface of the KCC-1 microspheres, and no obvious aggregation was observed. The lattice fringes are clearly visible with spacings of about 0.236 nm (Fig. 2d), corresponding to the lattice spacings of the (111) planes of Ag NPs [42].

3.2. Catalytic tests

The catalytic properties of the synthesized Ag/KCC-1 nanocatalyst were studied extensively by reduction reactions of 4-NP and 2-NA (Scheme 2). Both the reactions were easy to follow because of the formation of only one product in each case and the extent of the reaction was determined by measuring the change in UV–Vis absorbance [5,9,43–48]. As shown in Fig. 3a, pure 4-NP solution exhibites a distinct absorption maximum at 317 nm; however, the absorption peak shifted to 400 nm, immediately after the addition of $NaBH_4$ solution, corresponding to a color change from light to bright yellow due to the formation of 4-nitrophenolate ion in alkaline solution (Fig. 3a, *inset*). The maximum absorption at 400 nm did not change over time even after the addition of superfluous $NaBH_4$ solution confirming that the reduction did not proceed by aqueous $NaBH_4$ solution [49–51]. Furthermore, when the support KCC-1 was added to the 4-NP and $NaBH_4$ mixed solution, it was found that, the intensity of UV absorbance almost did not change, and the color of the 4-NP solution did not disappear even after 5 h (Figure S2), suggesting the KCC-1 support was almost inactive for the reduction reaction. The addition of Ag/KCC-1 nanocatalyst to 4-NP, led to the decrease in the peak intensity of 4-nitrophenolate ion at 400 nm with the concomitant increase in the peaks corresponding to 4-AP at 300 nm (Fig. 3b) reflecting the decay of 4-NP

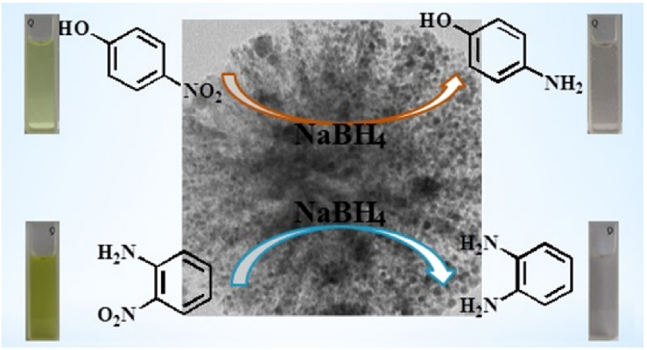

Scheme 2. The reduction of 4-NP and 2-NA on the surface of Ag/KCC-1 catalyst.

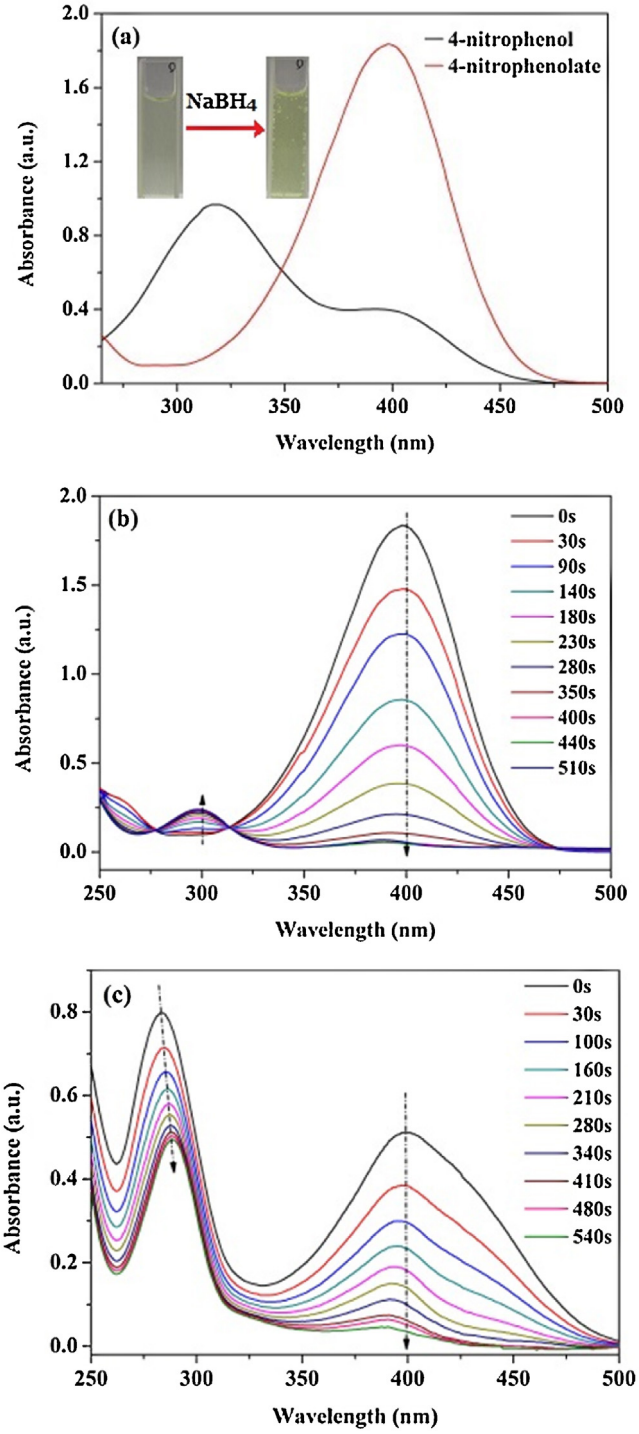

Fig. 3. UV–Vis spectra of 4-NP before and after adding $NaBH_4$ solution (a), the successive reduction of 4-NP to 4-AP (b) and 2-NA to o-PDA (c) over Ag/KCC-1 catalyst.

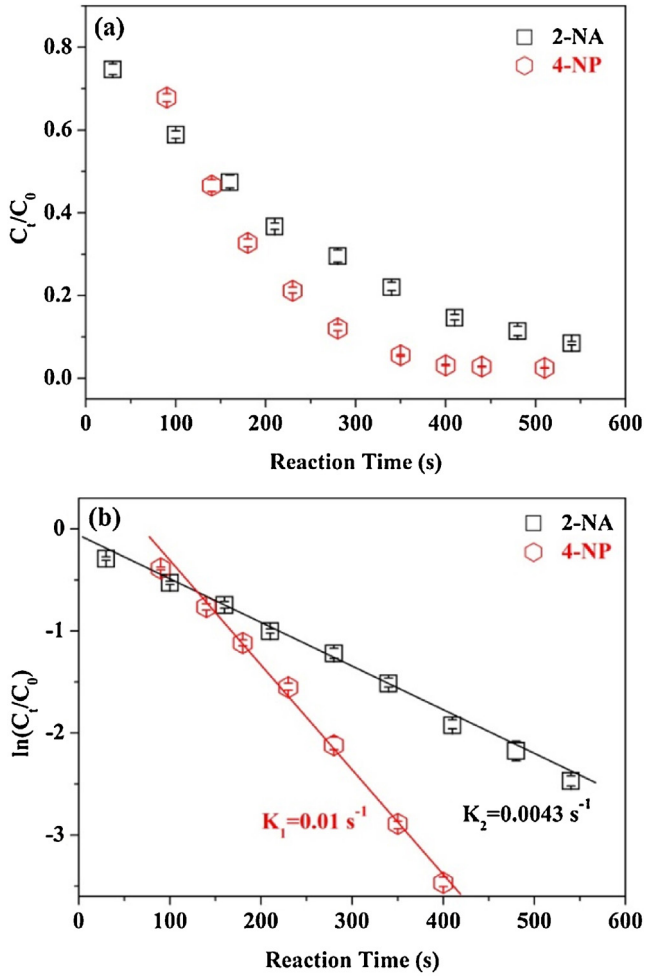

Fig. 4. Plots of C_t/C_0 (a) and $\ln(C_t/C_0)$ (b) versus reaction time for the reduction of 4-NP and 2-NA over Ag/KCC-1 catalyst.

and destruction of nitro group. The yellow colored solution of 2-NA exhibited two distinct absorption peaks at 282 and 400 nm, the intensity of the two peaks did not decrease with the addition of $NaBH_4$ solution. However, the intensity of the two peaks decreased gradually when adding Ag/KCC-1 nanocatalyst to 2-NA and $NaBH_4$ mixed solution (Fig. 3c).

Both the reduction reactions of 4-NP to 4-AP and 2-NA to *o*-PDA were completed within nine min and the yellow colored solutions became colorless after the completion of the reaction (Scheme 2). The catalytic performance of Ag/KCC-1 nanocatalyst for the reduction of 4-NP to 4-AP and 2-NA to *o*-PDA using $NaBH_4$ is depicted in Scheme 2. When 4-NP/2-NA and BH_4^- ions were adsorbed on the surface of Ag NPs of Ag/KCC-1 nanocatalyst, the reduction occurred via relaying of electrons from the donor BH_4^- to the acceptor 4-NP/2-NA [52].

The reaction conversion is calculated from C_t/C_0, measured in terms of the relative intensity of UV–Vis absorbance (A_t/A_0) at 400 nm. Herein, C_t is the concentration of 4-NP/2-NA at the reaction time t and C_0 is the initial concentration. Both the reduction reactions of 4-NP and 2-NA were repeated three times and the averaged values of the reaction conversions with standard deviation were given as shown in Fig. 4a. The concentration of $NaBH_4$ was significantly higher than that of 4-NP/2-NA in both the reduction reactions; thus, its concentration was considered as constant during the course of the reaction. Therefore, reduction reactions in both the cases were assumed to be pseudo first-order with respect to 4-NP/2-NA concentration [48,53]. As shown in Fig. 4b, the linear correlation between $\ln(C_t/C_0)$ and reaction time demonstrates that the reaction is of first-order with respect to the reduction of 4-NP/2-NA. Thus, the kinetic equation of this catalytic reduction reaction can be shown as $\ln(C_t/C_0) = -kt$, where k is the apparent first-order rate constant (s^{-1}), and t is the reaction time. The reaction rate constant k were calculated to be 1×10^{-2} and 4.3×10^{-3} s^{-1} for the Ag/KCC-1 catalyzed reduction of 4-NP and 2-NA, respectively. For a quantitative comparison, the activity parameter $k' = k/M$ was introduced, and defined as the ratio of the rate constant k to the weight of the catalyst added [1,52], where M is the total mass of the

Table 1
The comparison of catalytic activities for the reduction of 4-NP with catalysts reported in literatures.

Catalyst	Catalyst used (mg)	k (s^{-1})[a]	k/M (s^{-1} g^{-1})[b]
TAC-Ag-1.0 [54]	4.0	5.19×10^{-3}	1.3
Fe_3O_4-@SiO_2-Ag [55]	1.0	7.67×10^{-3}	7.67
Ag/C spheres [56]	1.0	1.69×10^{-3}	1.69
p(AMPS)-Ni [57]	50	9.38×10^{-4}	0.019
p(AMPS)-Co [58]	50	2×10^{-3}	0.04
p(AMPS)-Cu [59]	10	1.72×10^{-3}	0.172
Ag/KCC-1 (this work)	0.2	1×10^{-2}	50

[a] The reaction rate constant.
[b] The reaction rate constant per total weight of used catalyst.

catalyst added in the reaction. Thus, the reaction rate constants per unit mass were calculated to be 50 s^{-1} g^{-1} and 14.3 s^{-1} g^{-1} for the reduction of 4-NP and 2-NA, respectively.

The activity parameters used for the comparison of the catalytic activity of Ag/KCC-1 with the reported Ag NPs based catalysts employed for the reduction of 4-NP are listed in Table 1. According to the literature, TAC-Ag-1 [54] catalyst and the core–shell nanocomposite, Fe_3O_4@SiO_2-Ag [55] have the activity parameters of about 1.30 and 7.67 s^{-1} g^{-1}, respectively. The Ag doped carbon spheres have the rate constant k' of 1.69 s^{-1} g^{-1} [56]. The catalytic activity of Ag/KCC-1 nanocatalyst, obtained in this study, is 50 s^{-1} g^{-1} which is significantly higher than the catalytic activities of the abovementioned Ag based catalysts; thus Ag/KCC-1 nanocatalyst displayed superior catalytic activity for the reduction reactions. On the other hand, Nurettin Sahiner's group has reported non-noble metal modified hydrogel matrices catalysts for the reduction of 4-NP (Table 1) [57–59]. It can be seen from Table 1 that the rate constant k and activity parameter k′ of Ag/KCC-1 nanocatalyst are also higher than the reported p(AMPS)-Ni, p(AMPS)-Co and p(AMPS)-Cu catalysts. The excellent catalytic activity of Ag/KCC-1 nanocatalyst was attributed to its highly dispersed small-sized Ag NPs with easy accessibility of the active sites. Therefore, 4-NP/2-NA and BH_4^- were easily adsorbed on the surface of Ag NPs of Ag/KCC-1 nanocatalyst resulting in the rapid occurrence and completion of the reduction reactions.

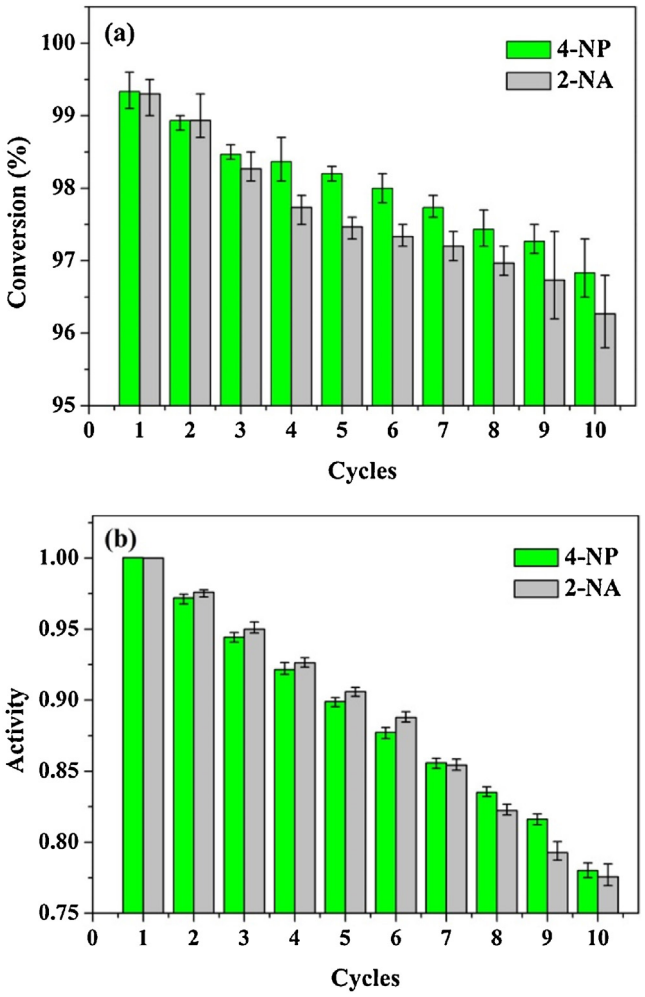

Fig. 5. The reusability (a) and activity (b) of Ag/KCC-1 catalyst for the reduction of 4-NP and 2-NA with $NaBH_4$.

For practical applications of heterogeneous systems, the level of reusability and the activity of the catalyst is an important factor. The reusability and the activity of the Ag/KCC-1 nanocatalyst were investigated in this study. The activity is calculated based on the reduction of the reaction rate relative initial rate for each use. After the completion of the catalytic reduction reactions of 4-NP and 2-NA, the used Ag/KCC-1 nanocatalyst was recovered by relay centrifugation and washed with water for the next catalytic run. Fig. 5a demonstrates that Ag/KCC-1 nanocatalyst undergoes an almost complete conversion during each cycle, not only for the reduction of 4-NP, but also for the reduction of 2-NA. Ag/KCC-1 nanocatalyst was reused for ten cycles for both the reduction reactions with a stable conversion of more than 96% within 10 min, which mainly attributed to the amino groups on the surface of KCC-1 nanospheres acted as robust anchors to prevent the aggregation and leaching of Ag NPs from the fibrous support. However, the activity of the Ag/KCC-1 nanocatalyst reduced to about 77% after ten cycles (Fig. 5b), this could be due to the poisoning of Ag catalyst via oxidation or catalyst inactivation.

4. Conclusions

In this study, novel fibrous KCC-1 based Ag/KCC-1 nanocatalyst with high surface area and sigificantly increased accessibility of the active sites, was successfully synthesized. Initially, KCC-1 was functionalized with amino groups which acted as robust anchors for the growth of the Ag NPs on the fibrous high surface area of KCC-1. Thus, Ag NPs with average diameter of about 4 nm were remarkably well-dispersed on the fibers of the KCC-1 microspheres without aggregation. The synthesized Ag/KCC-1 nanocatalyst exhibited excellent catalytic activity for the reduction of 4-NP and 2-NA in the presence of $NaBH_4$, owing to the easy accessibility of the nano support. Moreover, Ag/KCC-1 nanocatalyst was reused for at least ten cycles in both the reduction reactions with an almost complete conversion, mainly attributed to the prevention of leaching of Ag NPs from the fibrous support. Thus, the study of Ag/KCC-1 nanocatalyst may provide a potential platform for the fabrication of other noble metal nanocatalysts with easy accessibility, which would be highly efficient in various noble metal based catalytic reactions.

Acknowledgments

The authors acknowledge financial support from the NSFC (Grants 21301082), the Natural Science Foundation of Gansu (No. 1308RJYA028) and the Fundamental Research Funds for the Central Universities (lzujbky-2013-61).

Appendix A. Supplementary data

Supplementary data associated with this article can be found, in the online version, at http://dx.doi.org/10.1016/j.apcatb.2014.04.015.

References

[1] J. Zhang, G. Chen, M. Chaker, F. Rosei, D. Ma, Appl. Catal. B: Environ. 132 (2013) 107–115.
[2] F. Cardenas-Lizana, D. Lamey, N. Perret, S. Gomez-Quero, L. Kiwi-Minsker, M.A. Keane, Catal. Commun. 21 (2012) 46–51.
[3] Z.Y. Zhang, C.L. Shao, P. Zou, P. Zhang, M.Y. Zhang, J.B. Mu, Z.C. Guo, X.H. Li, C.H. Wang, Y.C. Liu, Chem. Commun. 47 (2011) 3906–3908.
[4] M. Zarejousheghani, M. Moeder, H. Borsdorf, Anal. Chim. Acta 798 (2013) 48–55.
[5] X. Li, X. Wang, S. Song, D. Liu, H. Zhang, Chem. Eur. J. 18 (2012) 7601–7607.
[6] F. Coccia, L. Tonucci, D. Bosco, M. Bressan, N. d'Alessandrro, Green. Chem. 14 (2012) 1073–1078.
[7] Y.C. Chang, D.H. Chen, J. Hazard. Mater. 165 (2009) 664–669.
[8] J.-R. Chiou, B.-H. Lai, K.-C. Hsu, D.-H. Chen, J. Hazard. Mater. 248 (2013) 394–400.
[9] Y. Zhang, X. Yuan, Y. Wang, Y. Chen, J. Mater. Chem. 22 (2012) 7245–7251.
[10] K. Li, Z. Zheng, X. Huang, G. Zhao, J. Feng, J. Zhang, J. Hazard. Mater. 166 (2009) 213–220.
[11] M.A. Oturan, J. Peiroten, P. Chartrin, A.J. Acher, Environ. Sci. Technol. 34 (2000) 3474–3479.
[12] O.A. O'Connor, L.Y. Young, Environ. Toxicol. Chem. 8 (1989) 853–862.
[13] M.S. Dieckmann, K.A. Gray, Water Res. 30 (1996) 1169–1183.
[14] H. Ozay, S. Kubilay, N. Aktas, N. Sahiner, Int. J. Polym. Mater. 60 (2011) 163–173.
[15] M. Muniz-Miranda, Appl. Catal. B: Environ. 146 (2014) 147–150.
[16] M.M. Mohamed, M.S. Al-Sharif, Appl. Catal. B: Environ. 142–143 (2013) 432–441.
[17] Y. Yang, Y. Guo, F. Liu, X. Yuan, Y. Guo, S. Zhang, W. Guo, M. Huo, Appl. Catal. B: Environ. 142–143 (2013) 828–837.
[18] N. Sahiner, N. Karakoyun, D. Alpaslan, N. Aktas, Int. J. Polym. Mater. Polym. Biomater. 62 (2013) 590–595.
[19] S. Saha, A. Pal, S. Kundu, S. Basu, T. Pal, Langmuir 26 (2010) 2885–2893.
[20] Y. Shiraishi, K. Fujiwara, Y. Sugano, S. Ichikawa, T. Hirai, ACS Catal. 3 (2013) 312–320.
[21] S. Paganelli, O. Piccolo, F. Baldi, R. Tassini, M. Gallo, G. La Sorella, Appl. Catal. A: Gen. 451 (2013) 144–152.
[22] P.J.C. Hausoul, S.D. Tefera, J. Blekxtoon, P.C.A. Bruijnincx, R.J.M.K. Gebbink, B.M. Weckhuysen, Catal. Sci. Technol. 3 (2013) 1215–1223.
[23] K. Imamura, T. Yoshikawa, K. Nakanishi, K. Hashimoto, H. Kominami, Chem. Commun. 49 (2013) 10911–10913.
[24] J.L. Long, H.L. Liu, S.J. Wu, S.J. Liao, Y.W. Li, ACS Catal. 3 (2013) 647–654.
[25] K. Suzuki, T. Yamaguchi, K. Matsushita, C. Iitsuka, J. Miura, T. Akaogi, H. Ishida, ACS Catal. 3 (2013) 1845–1849.
[26] H. Yotou, T. Okamoto, M. Ito, T. Sekino, S.I. Tanaka, Appl. Catal. A: Gen. 458 (2013) 137–144.
[27] M.L. Wang, T.T. Jiang, Y. Lu, H.J. Liu, Y. Chen, J. Mater. Chem. A 1 (2013) 5923–5933.
[28] H. Lee, S.E. Habas, S. Kweskin, D. Butcher, G.A. Somorjai, P. Yang, Angew. Chem. Int. Ed. 45 (2006) 7824–7828.
[29] J. Zeng, Q. Zhang, J. Chen, Y. Xia, Nano Lett. 10 (2010) 30–35.
[30] Y. Lin, Y. Qiao, Y. Wang, Y. Yan, J. Huang, J. Mater. Chem. 22 (2012) 18314–18320.
[31] X.D. Zhang, Z.P. Qu, F.L. Yu, Y. Wang, J. Catal. 297 (2013) 264–271.
[32] J.W. Zheng, H.Q. Lin, Y.N. Wang, X.L. Zheng, X.P. Duan, Y.Z. Yuan, J. Catal. 297 (2013) 110–118.
[33] N.S. Patil, R. Jha, B.S. Uphade, S.K. Bhargava, V.R. Choudhary, Appl. Catal. A: Gen. 275 (2004) 87–93.
[34] R.J. Pelaez, A. Castelo, C.N. Afonso, A. Borras, J.P. Espinos, S. Riedel, P. Leiderer, J. Boneberg, Nanotechnology 24 (2013).
[35] R.H. Liu, N.S. Gao, F. Zhen, Y.Y. Zhang, L. Mei, X.W. Zeng, Chem. Eng. J. 225 (2013) 245–253.
[36] D. Chen, Z. Qu, Y. Sun, K. Gao, Y. Wang, Appl. Catal. B: Environ. 142–143 (2013) 838–848.
[37] P.R. Selvakannan, K. Mantri, J. Tardio, S.K. Bhargava, J. Coll. Interf. Sci. 394 (2013) 475–484.
[38] A.M. Venezia, R. Murania, V. La Parola, B. Pawelec, J.L.G. Fierro, Appl. Catal. A: Gen. 383 (2010) 211–216.
[39] V. Polshettiwar, D. Cha, X. Zhang, J.M. Basset, Angew. Chem. Int. Ed. 49 (2010) 9652–9656.
[40] A. Fihri, D. Cha, M. Bouhrara, N. Almana, V. Polshettiwar, Chemsuschem 5 (2012) 85–89.
[41] X.G. Zhao, J.L. Shi, B. Hu, L.X. Zhang, Z.L. Hua, Mater. Lett. 58 (2004) 2152–2156.
[42] C. Dong, X. Zhang, H. Cai, J. Alloy Compd. 583 (2014) 267–271.
[43] J. Zheng, Y. Dong, W. Wang, Y. Ma, J. Hu, X. Chen, X. Chen, Nanoscale 5 (2013) 4894–4901.
[44] B. Xia, F. He, L. Li, Langmuir 29 (2013) 4901–4907.
[45] A. Shivhare, S.J. Ambrose, H. Zhang, R.W. Purves, R.W.J. Scott, Chem. Commun. 49 (2013) 276–278.
[46] K. Jiang, H.-X. Zhang, Y.-Y. Yang, R. Mothes, H. Lang, W.-B. Cai, Chem. Commun. 47 (2011) 11924–11926.
[47] F. Gonzalez de Rivera, I. Angurell, M.D. Rossell, R. Erni, J. Llorca, N.J. Divins, G. Muller, M. Seco, O. Rossell, Chem. Eur. J. 19 (2013) 11963–11974.
[48] H. Gu, J. Wang, Y. Ji, Z. Wang, W. Chen, G. Xue, J. Mater. Chem. A 1 (2013) 12471–12477.
[49] H. Wu, X. Huang, M.M. Gao, X.P. Liao, B. Shi, Green Chem. 13 (2011) 651–658.
[50] L.H. Qiu, Y.J. Peng, B.Q. Liu, B.C. Lin, Y. Peng, M.J. Malik, F. Yan, Appl. Catal. A: Gen. 413 (2012) 230–237.
[51] M.-Q. Yang, X. Pan, N. Zhang, Y.-J. Xu, Crystengcomm 15 (2013) 6819–6828.
[52] B. Baruah, G.J. Gabriel, M.J. Akbashev, M.E. Booher, Langmuir 29 (2013) 4225–4234.
[53] W. Hu, B. Liu, Q. Wang, Y. Liu, Y. Liu, P. Jing, S. Yu, L. Liu, J. Zhang, Chem. Commun. 49 (2013) 7596–7598.
[54] M.H. Rashid, T.K. Mandal, J. Phys. Chem. C 111 (2007) 16750–16760.
[55] Y. Chi, Q. Yuan, Y. Li, J. Tu, L. Zhao, N. Li, X. Li, J. Coll. Interf. Sci. 383 (2012) 96–102.
[56] S. Tang, S. Vongehr, X. Meng, J. Phys. Chem. C 114 (2009) 977–982.
[57] N. Sahiner, H. Ozay, O. Ozay, N. Aktas, Appl. Catal. A: Gen. 385 (2010) 201–207.
[58] N. Sahiner, H. Ozay, O. Ozay, N. Aktas, Appl. Catal. B: Environ. 101 (2010) 137–143.
[59] N. Sahiner, O. Ozay, Curr. Nanosci. 8 (2012) 367–374.